International Journal Of
Industrial Electronics Control and Optimization
Print ISSN: 3517-2645
Online ISSN: 3568-2645
Homepage: https://ieco.usb.ac.ir/

An Optimal Nonlinear Fractional Order Virtual Inertia Control Strategy for Islanded Microgrids with Renewables

Abbas-Ali Zamani[1,2]

Department of Electrical Engineering, National University of Skills (NUS), Tehran, Iran.[1]
Department of Electrical Engineering, Technical and Vocational University (TVU), Tehran, Iran.[2]
Corresponding author's email: a.zamani.edu@gmail.com

Article Info

Article type:
Research Article

Article history:
Received: 20-March-2025
Received in revised form: 02-May-2025
Accepted: 10-May-2025
Published online: 22-Dec-2025

Keywords:
Virtual Inertia,
Sustainable Energy Resources,
Nonlinear Fractional Order Controller,
Islanded Microgrid.

ABSTRACT

The large-scale integration of renewable generation into microgrids can lead to decreased inertia, resulting in high rates of change of frequency and frequency instability. This issue is even more complex in islanded MGs that incorporate a high proportion of RGs and need to deliver power to loads in islanded mode. To address this problem, a virtual inertia control scheme can be employed to enhance system inertia and maintain frequency stability. In this article, we propose a novel control strategy named the optimal nonlinear fractional-order PI-based virtual inertia controller, which integrates a nonlinear fractional-order PI controller into the conventional VIC loop. The designed ONFOPI+VI controller, which considers both inertia and damping properties, is optimized using the Coot optimization algorithm. Furthermore, an alternative control methodology, denoted as OFOPI+VI, has been developed to analyze and evaluate the outcomes obtained from the proposed ONFOPI+VI control structure. This paper compares the performance of the proposed ONFOPI+VI strategy to that of the OFOPI+VI and other VIC techniques for different RG and load variations under various scenarios. Simulation results and detailed analyses confirmed that the ONFOPI+VI controller significantly outperformed conventional methods, yielding at least a 30% improvement in IAE and a 20% improvement in ITAE compared to other control techniques.

I. Introduction

A. Virtual Inertia Control Background

In recent years, there has been a growing trend towards the integration of renewable generation (RG) into utility power systems. This shift is expedited in reaction to the adverse effects stemming from fossil fuel usage like environmental deterioration, global warming, and the consequences of greenhouse gas emissions [1-2]. The appeal of RGs lies in their clean, infinite, and cost-effective nature [3-4]. However, the inclusion of RGs into modern interconnected electricity networks can pose certain challenges and issues for utility grids. One such challenge is the diminished system inertia of interconnected electricity networks, which can be attributed to the use of power converters to interface RGs with the utility grid. Studies have shown that these converters can cause a drop in the inertia of the power system, leading to alterations in the frequency and voltage stability of the system [5]. The concept of virtual inertia (VI) control has been widely adopted in low inertia systems to enhance their inertia, as evidenced by previous studies [6-8].

B. Literature Review

One effective method for emulating the benefits of virtual inertia control (VIC) and improving system inertia is through the use of the derivative technique, as demonstrated in previous research [9]. For example, the application of this control methodology within interconnected power systems has demonstrated enhancements in frequency stability [3]. In a separate investigation [10], researchers introduced a VIC mechanism. This approach involves estimating the rates of change of frequency to effectively supply tailored inertia management for contingencies, thereby augmenting frequency stability in networks with limited inherent rotational inertia. Furthermore, a proportional-derivative control system was employed to improve the microgrid (MG) frequency stability in the presence of PV arrays [11].

Besides this approach, a range of VIC mechanisms have been deployed with the objective of fortifying frequency

stability. Based on several review papers, such as [12-14], various VIC techniques have been proposed for low inertia systems, including droop control, hidden inertia emulation, and energy storage integration. For example, the utilization of a blend of fuzzy interval-type-2 and proportional integral controllers in islanded microgrids has been investigated [15]. Equilibrium optimization is employed in this study to fine-tune controller parameters. In [16], VIC methods were classified into energy storage-based and non-energy storage-based techniques. Some researchers have proposed specific VIC schemes for certain systems, such as a VI and frequency control scheme for wind power-based systems [17] and VI control techniques for improving dynamic stability in microgrids [18]. Other studies have explored derivative-type VIC using different controllers, such as PSO-optimized Proportional-Integral (PI) controllers [19], Genetic Algorithm (GA)-based PI controllers [20], fuzzy logic controllers [21], and H-infinity controllers [21, 22]. Some of the previous studies [17-19, 21] have not incorporated the damping constant component in their design of the VI control system. As a consequence, the frequency response exhibits sub-optimal dynamic characteristics characterized by elevated peak values and prolonged settling times.

The appeal of the Fractional Order Controller (FOC) family has attracted many researchers, particularly in the realm of power system control [23-27]. The application of FOCs extends to the domain of VI control. For instance, in a study denoted as [28], researchers explored the efficacy of fractional-order controllers within a modern power grid incorporating solar photovoltaic plants (SPP), wind power plants (WPP), and a thermal unit. The study utilized the flower pollination algorithm as an efficient method to finely tune the controller. In another investigation, a Fractional Order (FO) integral-based control strategy, incorporating VIC, was deployed in a multi-area electricity network [29]. Despite achieving commendable results, it is noteworthy that the damping effect of virtual inertia was not included in this particular reference. Subsequently, in a separate study, a genetic algorithm-optimized FO controller was introduced to enhance the stability of modern power systems featuring RGs [30]. However, none of these studies [28-30] have utilized nonlinear fractional order controllers as the designed controllers in the VIC loops.

C. Motivation and Research Gap

One of the primary challenges in microgrids with renewable energy sources (RESs) is maintaining frequency stability. Despite the advancements in virtual inertia control, several aspects of this issue still require further investigation. In particular, it has become clear that the control gains of virtual inertia significantly influence the power flow in and out of Energy Storage Systems (ESSs), which in turn has a profound impact on the stability of the MG and its ability to respond to disturbances. Therefore, optimizing these control parameters is critical to ensure system stability and performance.

Additionally, many existing studies overlook the importance of integrating into VIC systems. The absence of Virtual Damping (VD) can lead to suboptimal power flow in ESSs and diminish the effectiveness of VI control, especially in MGs where the inherent inertia and damping are constrained. Conventional PI controllers, although widely applied, face limitations in inverter-based ESSs. These controllers struggle to replicate the behavior of synchronous generators or emulate synthetic inertia in MGs. The intermittent nature of renewable generation and the variability in load conditions further exacerbate the performance issues of PI controllers. Moreover, these controllers often encounter difficulties in maintaining system stability under uncertain conditions.

In response to these challenges, non-linear control theories, including non-linear fractional-order control methods, have emerged as viable solutions. Traditional linear control methods, though often employed due to their mathematical simplicity, are limited to specific operational points where linearization is feasible. However, many real-world systems, particularly power systems, exhibit inherent non-linearities that demand more advanced control strategies. Non-linear techniques, such as reset control, sliding mode control, and non-linear PID control, are increasingly being considered. Among these, fractional calculus stands out as an effective approach for dealing with the complexities of control engineering.

Given the inherent non-linearity of modern power systems and the growing complexity introduced by high penetration of renewable generation, there is a clear need for innovative control solutions. Non-linear fractional-order control represents an interdisciplinary field that combines the mathematical intricacies of non-linearity and fractional calculus, offering a departure from traditional control paradigms [31, 32]. This approach has the potential to address the persistent challenges in VIC, particularly in low-inertia, islanded MGs.

Upon reviewing the existing literature on VIC, it is evident that various controllers have been employed to improve the stability of MGs. However, significant gaps remain, particularly regarding the integration of VD and the use of nonlinear fractional-order controllers in VIC systems. Given the uncertainties and non-linearities of today's electrical networks, exacerbated by the intermittent nature of renewable generation, this study introduces the Optimal Nonlinear Fractional-Order PI-based Virtual Inertia (ONFOPI+VI) methodology as a promising solution. This approach aims to enhance control performance and stability in low-inertia, islanded MGs, thereby addressing critical control challenges in modern microgrid systems.

D. Contribution

In the pursuit of heightened MG stability, this research introduces a novel VIC configuration, employing an Optimal Nonlinear Fractional Order Proportional-Integral (NFOPI) controller. This technique enhances control performance, stability, and robustness even in the presence of nonlinearities and uncertainties. While the configuration takes into account both virtual inertia and virtual damping for VI emulation, the proposed ONFOPI+VI framework incorporates the Coot Optimization Algorithm (COA) to determine optimal VI parameters, integral order, as well as gains for the ONFOPI. The method's flexibility ensures that VI, damping, and ONFOPI parameters are precisely set to the specific system conditions, thereby enhancing stability and performance amidst power oscillations. As opposed to customary control methodologies, this technique allows for optimal adjustments to controller and damping sizes. The ability of the proposed framework to control nonlinear systems and the optimal gain utilization enables the controller to effectively respond to system changes in the presence of nonlinearities and uncertainties.

The contributions of this article can be summarized as follows:

•Introduction of a new control mechanism, ONFOPI+VI, tailored for VIC emulation in islanded microgrids with a significant RG share.

•Consideration of both inertia and damping components in the VIC system within the control system model.

•Determination of optimal values for VIC system parameters, including inertial and derivative gains, as well as NFOPI controller gains and its non-integer orders, using the COA.

•Design and comparison of an alternative control strategy, Optimal Fractional-Order PI-based Virtual Inertia (OFOPI+VI), integrating Fractional Order Proportional-Integral (FOPI) into the VIC loop.

•Proposition of various scenarios to assess the functionality of the proposed control framework, evaluating their efficacy over a broad spectrum of load and generation variations.

•The superior performance of the proposed ONFOPI+VI over the traditional VI (T-VI), COA-optimized VI (COA-VI), GA-optimized PI-based VI (GAPI+VI), and OFOPI+VI are demonstrated.

The T-VI and GAPI+VI controllers from [15, 20] were employed for comparative analysis.

The upcoming sections of this research manuscript are structured as follows: Section 2 provides an extensive introduction to the model of the microgrid being studied. In Section 3, we present a summary of the virtual inertia control mechanism, whereas Section 4 delves into the innovative virtual inertia control system introduced in this investigation. Section 5 comprehensively presents the numerical findings, and lastly, Section 6 furnishes a conclusive summary of the outcomes.

II. Modeling of the Islanded Microgrid

To assess the efficacy of the proposed ONFOPI+VI controller, a thorough examination is carried out on a disconnected MG. The MG configuration consists of varied elements, incorporating a thermal power plant and RGs such as WPPs and SPPs, as indicated in Fig. 1. The studied MG is comprised of a 20 MW thermal power generation (TPG), an 8 MW WPP, a 4 MW SPP, a residential demand of 5 MW, and a 10 MW industrial power consumption. The baseline power of the grid is established at 20 MW, as outlined in previous works [15, 19, 20].

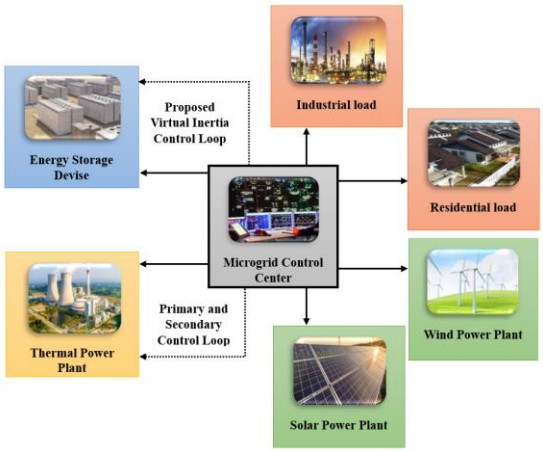

Fig. 1. Diagram of depicting the analyzed islanded microgrid

Fig. 2 illustrates the dynamic model of the microgrid that is currently being investigated [15, 20, 26, 28, 33]. The model comprises block diagrams of a typical frequency control study, which includes the Generator Rate Constraint (GRC) for the governor unit and the rate limitation of the turbine-valve/gate closing or opening speed (V_U, V_L) for the turbine unit. The GRC value was estimated to be 20% P.U. MW/min in this study. Appendix 1 lists the parameters of the microgrid system that was studied [15, 20].

Taking into account the inertia, primary and secondary control, as well as the dynamic effects of the generations and loads shown in Fig. 2, The variation in frequency and fluctuations in the power of the RGs is obtained as follows [33]:

$$\Delta f(s) = \frac{1}{2Hs + D}\left(\Delta P_m(s) + \Delta P_W(s) + \Delta P_{PV}(s) + \Delta P_{VI}(s) - \Delta P_L(s)\right) \quad (1)$$

in this equation:

$$\Delta P_m(s) = \frac{1}{1 + sT_t}\Delta P_g(s) \quad (2)$$

$$\Delta P_g(s) = \frac{1}{1 + sT_g}\left(\Delta P_C(s) - \frac{1}{R}\Delta f(s)\right) \quad (3)$$

$$\Delta P_C(s) = \frac{K_S}{s}(\beta \cdot \Delta f(s)) \quad (4)$$

$$\Delta P_W(s) = \frac{1}{1+sT_{WT}}\Delta P_{\text{wind}}(s) \quad (5)$$

$$\Delta P_{PV}(s) = \frac{1}{1+sT_{PV}}\Delta P_{\text{solar}}(s) \quad (6)$$

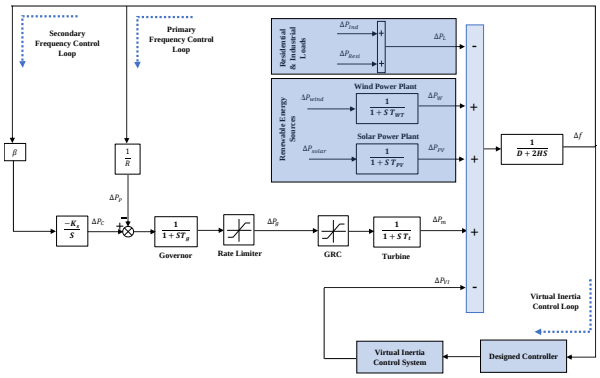

Fig. 2. The dynamic model of the MG under study

In the presented equations, the variables are defined as follows: P_C represents changes in the area control error action resulting from secondary control, ΔP_m denotes fluctuations in the output power of the TPG, ΔP_P signifies variations in the primary control's control action, ΔP_W accounts for fluctuations in the generated power from the WPP, ΔP_{wind} characterizes changes in the initial wind power, ΔP_g indicates the generated power from turbines, ΔP_{solar} represents alterations in the initial solar energy level, ΔP_{PV} captures fluctuations in the generated power from the SPP, ΔP_{Ind} signifies alterations in the demand from industries, ΔP_{Resi} denotes shifts in residential load power usage, ΔP_L denotes the overall shift in the system's load profile, and ΔP_{VI} accounts for shifts in the output power of the VI module.

III. Virtual Inertia Mechanism

In traditional electricity networks, the stability of the electricity grid is maintained by the kinetic energy stored in the rotational mass of traditional generators, which provides the network's inertia. However, in islanded MGs, RGs are tasked with delivering electricity power to the demand side. With the increasing adoption of inverter-connected RGs into MGs characterized by limited inertia, the system inertia is reduced, which can lead to instability and cascading failures in frequency events. To address this issue, VIC can be employed in low-inertia MGs to emulate the inertia of conventional generation units. In this paper, virtual damping and virtual inertia control as depicted in Fig. 3, which have been utilized in many investigations [15, 20, 30, 33], are considered for the energy storage system to calculate the ESS active power and add it to the target value for the microgrid in the event of disturbances. By employing VIC in the ESS, the requisite VIC power can be provided to strengthen the stability of grid frequency. The equation for VIC is expressed as:

$$\Delta P_{VI}(s) = \frac{sK_{VI}+D_{VI}}{1+sT_{INV}}(\Delta f(s)) \quad (7)$$

In this equation, K_{VI} is the Virtual inertia gain and D_{VI} indicates the Virtual damping gain.

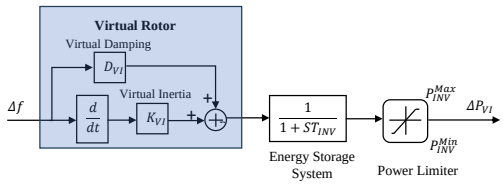

Fig. 3. Virtual inertia control mechanism.

IV. The designed procedures of the proposed control strategies

In this part, we will present three distinct control approaches for simulating inertia in the MG. These approaches consist of the innovative ONFOPI+VI controller, which is the main contribution of this article, along with the optimal COA-VI and the OFOPI+VI control strategies. We will use the COA-VI and OFOPI+VI control strategies for analyzing and comparing the findings.

A. Optimal Design of VIC Using the COA

We first designed the COA-VI controller for the MG system. The block diagram of the proposed COA-VI controller is shown in Fig. 4. In this approach, the parameters of the VIC are optimally tuned using the COA.

With regard to the cost function as per Equation (8) and the θ_v^{VI} VI's designing array, the parameters of optimal VI will be devised.

$$C_f(\theta_v^{VI}) = \int_{t=0}^{T_f} t|\Delta f|\,dt \quad (8)$$

$$\theta_v^{VI} = [\mathrm{K_{VI}\ D_{VI}}]^{\mathrm{T}} \quad (9)$$

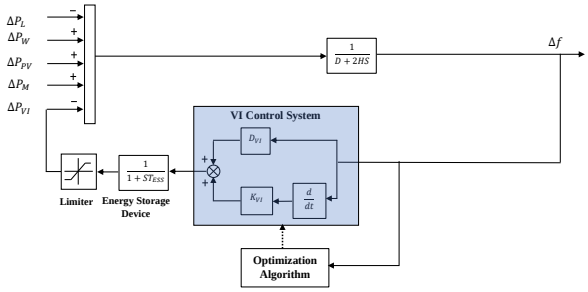

Fig. 4. The block diagram of COA-VI control structure.

The design vector is constrained within the bounds of $0 \leq K_{VI} \leq 5$ and $0 \leq D_{VI} \leq 5$. To minimize the objective function presented in Equation (8) and determine the optimal VI gains, the COA is employed. The COA, originally proposed by Naruei and Keynia [34], draws inspiration from the collective behavior of coots, a type of waterfowl. This algorithm aims to replicate both the regular and irregular movements observed in coots on the water's surface. The stages of the COA can be succinctly outlined as follows [34]:

Step1: The population is first randomly generated using the equation:

$$Cootpos\ (i) = rand\ (1, d) * (ub - lb) + lb \quad (10)$$

in which $Cootpos\ (i)$, d, ub, and lb refer to the position of i^{th} coot, the number of decision variables, and the upper and lower bands of search space, respectively.

Step 2: For each coot location, the cost function is calculated. Additionally, the parameters N_L and N_{coot}, denoting the number of leaders and coots, are randomly selected to identify the best coot or leader as the global optimum.

Step 3: In this stage, the coots' locations are then updated through four movements:

A. *Random movement of the swarm to both sides:*

Firstly, a stochastic location Q is produced using the equation:

$$Q = rand\ (1, d) * (ub - lb) + lb \quad (11)$$

To prevent being trapped in local optima, this location is updated as outlined below:

$$\text{Cootpos}\ (i) = \text{Cootpos}\ (i) + \Lambda_{cootpos} * R_2 * (Q - \text{Cootpos}\ (i)) \quad (12)$$

$$\Lambda_{cootpos} = 1 - iter * \left(\frac{1}{maxiter}\right) \quad (13)$$

In the above equation, R_2 refers to a random number in the interval [0,1] and $iter$ and $maxiter$ are the current interaction and the maximum iteration, respectively.

B) Chain Movement

To simulate this movement, the average position of two coots is obtained using Eq. (14).

$$Cootpos\ (i) = 0.5 * (Cootpos\ (i-1) + Cootpos\ (i)) \quad (14)$$

C) Location Adjustment Based on the Leaders of the Group.

As the coots navigate, they align their positions with the group leaders. This entails adapting their positions according to the leaders of the group. Denoting K as the leader's index number, i as the index number of the current coot, and N_L as the total number of leaders, the coot's selection of a leader can be expressed as outlined below:

$$K = 1 + (i\ MOD\ N_L) \quad (15)$$

In the above-mentioned movement, the position of coots is updated as follows:

$$Cootpos\ (i) = Leaderpos\ (k) + 2 * R_1 * cos\ (2\pi R) * (Leaderpos\ (k) - Cootpos\ (i)) \quad (16)$$

in which R_1 is a random number in the interval [0,1]. Also, $Leaderpos\ (k)$ and R are chosen leader locations and a stochastic number in the interval [-1,1], respectively.

D) Leader movement

To converge towards the optimal region, the group leader's location is updated according to Equation (17)

$$Leaderpos(i) = \begin{cases} B_{cootpos} * R_3 * \cos(2\pi R) * \\ \left(gbest - Leaderpos(i)\right) + gbest,\ R_4 < 05 \\ B_{cootpos} * R_3 * \cos(2\pi R) * \\ \left(gbest - Leaderpos(i)\right) - gbest,\ R_4 \geq 05 \end{cases} \quad (17)$$

$$B_{cootpos} = 2 - iter * \left(\frac{1}{maxiter}\right) \quad (18)$$

here, R_3 and R_4 are the stochastic numbers in the interval [0,1] and $gbest$ is the position ever found.

Step 4: Achieving Algorithm Convergence by Increasing Iterations.

Increasing the number of iterations leads to the discovery of the best cost function and ensures the convergence of the algorithm.

B. *The Design Procedure of the Proposed FOPI-Based VI Controller*

In this section, at first, the preliminaries of the fractional order PI controller are presented, and then the design procedure of the designed FOPI-based VI controller is described.

Initially, the OFOPI+VI controller is implemented to replace the inertia necessary for the electricity network. This framework is meticulously crafted in accordance with frequency and power control criteria. It's essential to highlight the significance of VI parameters and FOPI coefficients in ensuring the stability of microgrids and their ability to handle disturbances effectively. Consequently, fine-tuning these gains becomes paramount for achieving optimal functionality. The OFOPI+VI control strategy leverages the COA algorithm to find the optimum values of VI and FOPI gains, K_{VI}, D_{VI}, K_P, K_I, and λ.

B.1. Preliminaries of Fractional Order Controller

Combining differentiation with the fundamental non-integer order operator, defined as follows, results in fractional calculus.

$${}_aD_t^{\beta} = \begin{cases} \frac{d^{\beta}}{dt^{\beta}} & \beta > 0 \\ 1 & \beta = 0 \\ \int_a^t (d\tau)^{\beta} & \beta < 0 \end{cases} \quad (19)$$

In Equation (19), the operation's bounds are a and t, while its order is determined by β ($\beta \epsilon R$). Several methods, such as

Grunwald-Letnikov, Riemann-Liouville, and Caputo, can be used to represent fractional integro-differential equations. However, Caputo's formula is the most widely used approximation for this purpose, and it is given by the following equation.

$$D^{\alpha}f(t) = \frac{1}{\Gamma(m-\alpha)}\int_0^t \frac{D^m f(t)}{(t-\tau)^{\alpha+1-m}}d\tau, \alpha \in R^+, m \in Z^+, m-1 \le \alpha \le m \quad (20)$$

where α represents the order of the derivative of f(t) with zero initial conditions, and Γ(·) denotes the Gamma function.

Oustaloup [35] was a pioneer in applying FOC for dynamic system control, leading to the development of the CRONE controller (a French acronym for Commande Robuste d'Ordre Non-Entier). His studies demonstrated that this controller outperforms the classical PID controller in various applications. On the other hand, Podlubny [36] introduced the FOPID controller as an extension of the PID controller. This controller exhibits strong performance in both the time and frequency domains. The FOPID controller provides greater flexibility by incorporating non-integer orders for integration and differentiation, allowing for more accurate adjustments. In contrast to traditional PID controllers, FOPID can more effectively model systems with complex dynamics. This results in better transient performance, enhanced stability under parameter changes, and improved frequency regulation in microgrids. The following equations present the output expressions for PID and FOPID controllers in the time domain.

$$u_{PID}(t) = K_P e(t) + K_I \int_0^t e(\tau)\,d\tau + K_D \frac{de(t)}{dt} \quad (21)$$

$$u_{FOPID}(t) = K_P e(t) + K_I D^{-\lambda} e(t) + K_D D^{\mu} e(t) \quad (22)$$

In these equations, K_P, K_I, and K_D represent the gains associated with the proportional, integral, and derivative terms, respectively. The parameters λ and μ define the orders of the integral and derivative operators. The function e(t) denotes the error, which is the difference between the desired reference value and the actual system output. Unlike conventional PID controllers, the FOPID controller introduces two additional tuning parameters, making the adjustment process more complex.

B.2. The Design Procedure of the Designed OFOPI+VI Control Methodology

In this paper, the fractional order PI controller as described in the following equation is used to improve the performance of the VIC.

$$u_{FOPI}(t) = K_P e(t) + K_I D^{-\lambda} e(t) \quad (23)$$

The block diagram of the proposed OFOPI+VI controller is depicted in Fig. 5.

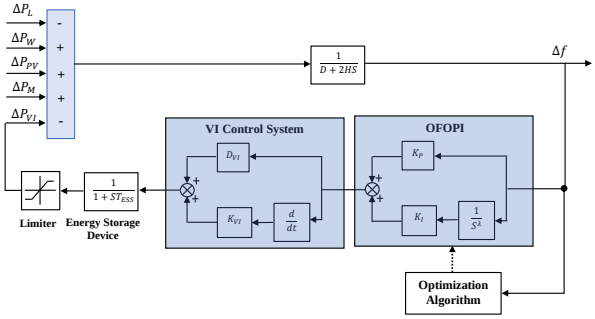

Fig. 5. The schematic diagram of OFOPI+VI controller.

Taking into account the cost function outlined in the previous section, the design procedure utilizes the following design vector:

$$\theta_v^{VI} = [\mathrm{K_P}\ K_\mathrm{I}\ \lambda]^\mathrm{T} \quad (24)$$

The upper and lower bounds of the design vector are defined as $0 \le K_P \le 200, 0 \le K_I \le 200$, and $0 \le \lambda \le 2$, respectively.

C. The Design Procedure of the Proposed Nonlinear Fractional-Order PI-Based VI Controller

In this section, at first, the preliminaries of the nonlinear fractional order PI controller are presented, and then the design procedure of the proposed ONFOPI+VI controller is described.

C.1. Preliminaries of Nonlinear Fractional Order Controller

The Nonlinear Fractional-Order Controller (NFOC) was introduced by Petras [32, 37-38]. Through various examples, he demonstrated the effective performance of NFOC in nonlinear control systems. The output expression for the nonlinear FOPID controller is given as follows:

$$u_{NFOPID}(t) = g\big(e(t)\big)\Big(K_P e(t) + K_I D^{-\lambda} e(t) + K_D D^{\mu} e(t)\Big) \quad (25)$$

$$g\big(e(t)\big) = K_0 + (1-K_0)|e(t)|\ , \qquad K_0 \epsilon (0,1) \quad (26)$$

When $K_0 = 1.0$, the classical form of the FOPID controller in Eq. (22) is obtained. However, when $K_0 \neq 1.0$, the system defines a nonlinear FOPID controller with six degrees of freedom.

C.2. The Design Procedure of the Proposed ONFOPI+VI Controller

In this section, the nonlinear fractional order PI controller as described in the following equation is used to improve the performance of the optimal COA-VI designed in section A.

$$u_{NFOPI}(t) = g(\Delta f)\big(K_P \Delta f + K_I D^{-\lambda} \Delta f\big) \quad (27)$$

$$g(\Delta f) = K_0 + (1-K_0)|\Delta f|\ , \qquad K_0 \epsilon (0,1) \quad (28)$$

The block diagram of the proposed ONFOPI+VI controller is depicted in Fig. 6.

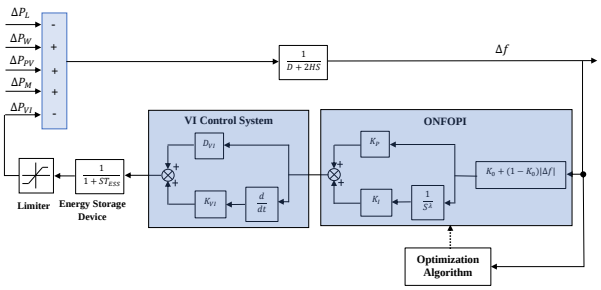

Fig. 6. The schematic diagram of the ONFOPI+VI controller.

Using the cost function of relationship (8), the following design vector is used for the design procedure.

$$\theta_v^{VI} = [\mathrm{K}_P\ K_\mathrm{I}\ \ K_0\ \ \lambda]^\mathrm{T} \tag{29}$$

The upper and lower bounds of the design vector are $0 \leq K_P \leq 200$, $0 \leq K_I \leq 200$, $0 \leq K_0 \leq 1$ and $0 \leq \lambda \leq 2$, respectively.

V. Results, Analysis, and Discussion.

This section examines the significance and efficiency of implementing the suggested ONFOPI+VI to enhance the grid's frequency response. The industrial and residential loads were simulated using the signal builder block, as shown in Fig. 2. The TPG has been modeled using first-order transfer functions, GRC, and limiter blocks. Additionally, the WT and PV systems have been simulated using first-order transfer function blocks. The ESS modeling has been presented using first-order transfer function blocks. To demonstrate the effectiveness of the proposed inertia control design, nonlinear simulations have been conducted using MATLAB/Simulink software. These simulations involve contrasting critical cases with different penetration rates of RGs and load patterns to examine the microgrid frequency response. In this research article, we evaluate the performance of different VI controller strategies in three different cases. We use *Δf*, as an indicator to assess the grid's functionality.

In power system stability assessment, four principal performance indicators are typically utilized: the Integral Square Error (ISE), Integral Absolute Error (IAE), Integral Time Weighted Absolute Error (ITAE), Maximum Overshoot (MO), and Maximum Undershoot (MU). These metrics have become standard evaluation tools in dynamic system studies, defined mathematically as follows:

$$IAE = \int_{t=0}^{t=T_{sim}} |\Delta f|\, dt \tag{30}$$

$$ISE = \int_{t=0}^{t=T_{sim}} (\Delta f)^2\, dt \tag{31}$$

$$ITAE = \int_{t=0}^{t=T_{sim}} t|\Delta f|\, dt \tag{32}$$

$$MO = max(f(t)) - f_{nominal} \tag{33}$$

$$MU = f_{nominal} - min(f(t)) \tag{34}$$

The comparative analysis shows that the ONFOPI+VI control methodology outperforms other control approaches. Specifically, the ONFOPI+VI controller yielded better outcomes than the T-VI, COA-VI, GAPI+VI, and OFOPI+VI control methods, resulting in an enhanced frequency response. The results yielded from utilizing the COA algorithm to the OFOPI+VI controllers in comparison with those of the T-VI and GAPI+VI are shown in Table 1. Furthermore, Table 2 displays the characteristics of the ONFOPI-based VI controller tailored for the assessed MG. The swarm size and the maximum iterations of the COA algorithm for COA-VI, OFOPI+VI, and ONFOPI+VI are selected as 500 and 100, respectively.

TABLE I PARAMETERS OF T-VI, COA-VI, GAPI+VI, AND OFOPI+VI CONTROLLERS PERTAINING TO THE EVALUATED MG

Control Method	K_P	K_I	K_{VI}	D_{VI}	λ
W-VI	-	-	-	-	-
T-VI	-	-	0.5	-	-
COA-VI	-	-	2.962	3.862	-
GAPI+VI	113.663	122.14	3.710	4.794	-
OFOPI+VI	136.412	142.677	2.962	3.862	0.865

TABLE II PARAMETERS OF THE DEVELOPED ONFOPI+VI CONTROLLER FOR THE MG UNDER EXAMINATION

	K_P	K_I	K_{VI}	D_{VI}	λ	K_0
ONFOPI+VI Controller	197.101	189.962	2.962	3.862	0.585	0.895

A. Case I: Dynamic Response of the MG to Sever Load Changes

This subsection presents the results of Case I, which investigates the impact of connecting and disconnecting various loads in the presence of RGs. In this case, the residential load ΔP_{Resi} was disconnected after 40 seconds at a level of 0.05. The industrial load ΔP_{Ind} became grid-connected after 20 seconds at a level of 0.1. The generation from the W_{PP} had an initial change ΔP_W of 0.12 from the beginning, while the generation from the SPP also had an initial change ΔP_{PV} of 0.08 from the start. It is worth mentioning that all changes are in P.U. Table 3 summarizes the different operational conditions studied in Case I.

The changes in frequency deviation for this scenario are shown in Fig.7 and Table 4. These results indicate that the ONFOPI+VI control method is better than the T-VI, COA-VI, GAPI+VI, and OFOPI+VI methods.

B. Case II: Dynamic Response of the MG to Sever Changes of Different RGs

At the outset, the residential load undergoes a 0.05 change, whereas the industrial load sees a 0.1 increase. The

TABLE III OPERATIONAL CONDITIONS UNDER CASE I.

	Connecting	Disconnecting	(P.U.)
ΔP_{Resi}	$0s$	$40s$	0.05
ΔP_{Ind}	$20s$	-	0.1
ΔP_W	$0s$	-	0.12
ΔP_{PV}	$0s$	-	0.08

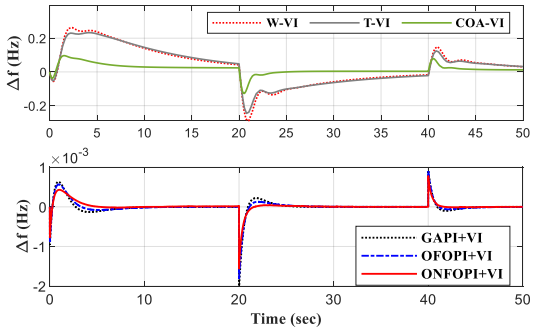

Fig. 7. Performance comparison of T-VI, COA-VI, GAPI+VI, OFOPI+VI, and proposed ONFOPI+VI control frameworks for the microgrid under examination pertaining to Case I

TABLE IV EVALUATING THE PERFORMANCE OF VARIOUS CONTROL METHODOLOGIES FOR THE MICROGRID IN CASE I.

Control Method	IAE	ISE	ITAE	MU	MO
W-VI	4.8268	0.7068	87.378	-0.2903	0.2625
T-VI	4.7372	0.6425	86.142	-0.2457	0.2326
COA-VI	1.1904	0.0573	20.180	-0.1279	0.0963
GAPI+VI	0.0032	2.00e-06	0.0522	-0.0021	0.0010
OFOPI+VI	0.0031	2.00e-06	0.0475	-0.0021	0.0010
ONFOPI+VI	0.0022	1.00e-06	0.0319	-0.0015	0.0008

generation from the WPP changes by 0.12 but is disconnected after 40 seconds. Meanwhile, the input from the SPP experienced a 0.08 change after 20 seconds, when it became grid-connected. Table 5 summarizes the different operational conditions studied in Case II.

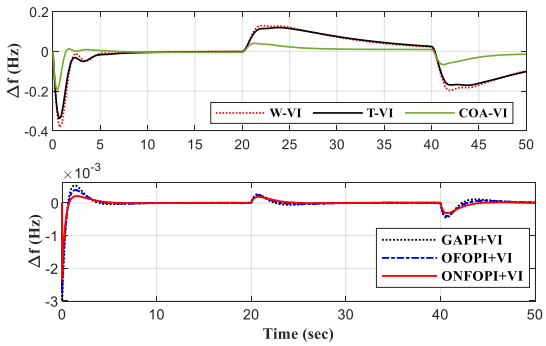

i) Performance comparison of T-VI, COA-VI, GAPI+VI, OFOPI+VI, and proposed ONFOPI+VI control frameworks for the microgrid under examination pertaining to Case II

TABLE V OPERATIONAL CONDITIONS UNDER CASE II.

	Connecting	Disconnecting	(P.U.)
ΔP_{Resi}	$0s$	-	0.05
ΔP_{Ind}	$0s$	-	0.1
ΔP_W	$0s$	$40s$	0.12
ΔP_{PV}	$20s$	-	0.08

TABLE VI EVALUATING THE PERFORMANCE OF VARIOUS CONTROL METHODOLOGIES FOR THE MICROGRID IN CASE II

Control Method	IAE	ISE	ITAE	MU	MO
W-VI	3.4333	0.4896	104.234	-0.3814	0.1293
T-VI	3.3563	0.4274	101.886	-0.3382	0.1195
COA-VI	0.8721	0.0427	23.864	-0.1930	0.0405
GAPI+VI	0.0033	2.0e-06	0.0566	-0.0031	0.00054
OFOPI+VI	0.0032	2.0e-06	0.0529	-0.0027	0.00039
ONFOPI+VI	0.0023	1.0e-06	0.0419	-0.0024	0.00021

The changes in frequency deviation for this scenario are shown in Fig.8 and Table 6. These results indicate that the ONFOPI+VI control method is better than the T-VI, COA-VI, GAPI+VI, and OFOPI+VI methods.

C. Case III. Dynamic Response of the MG to Sever and Simultaneous Changes of Different Types of Loads and RGs

In Case III, various components undergo changes in power supply and demand. The residential load disconnects by 0.05 at 65 seconds, while the industrial load connects by 0.1 after 25 seconds. The WPP connects by 0.12 after 45 seconds. Concurrently, the SPP disconnects by 0.08 at 85 seconds. Table 7 summarizes the different operational conditions studied in Case III. The changes in frequency deviation for this scenario are shown in Fig.9 and Table 8.

TABLE VII OPERATIONAL CONDITIONS UNDER CASE III.

	Connecting	Disconnecting	(P.U.)
ΔP_{Resi}	$0s$	$65s$	0.05
ΔP_{Ind}	25 s	-	0.1
ΔP_W	$45s$	-	0.12
ΔP_{PV}	$0s$	$85s$	0.08

In Case III, the ONFOPI+VI stands out among four other controllers (W-VI, T-VI, GAPI+VI, and OFOPI+VI) regarding MO, MU, ISE, ITAE, and IAE. In particular, the ONFOPI+VI makes significant strides, with roughly 99.60% better performance contrasted with the T-VI control methodology, 99.17% contrasted with the COA-VI controller, 30.00% contrasted with the GAPI+VI controller, and 30.00% contrasted with the OFOPI+VI control methodology in terms of MO. Regarding MU, the ONFOPI+VI demonstrates significant enhancements of around 99.43% contrasted with the T-VI, 98.92% contrasted

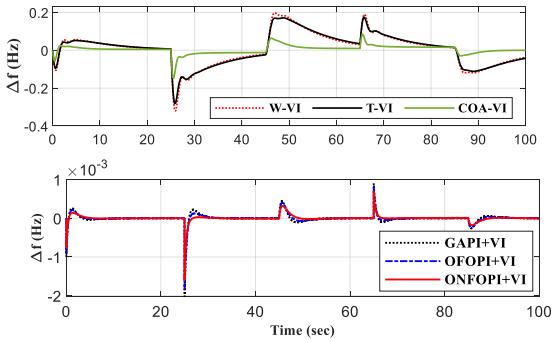

Fig. 8. Performance comparison of T-VI, COA-VI, GAPI+VI, OFOPI+VI, and proposed ONFOPI+VI control frameworks for the microgrid under examination pertaining to Case III

TABLE VIII EVALUATING THE PERFORMANCE OF VARIOUS CONTROL METHODOLOGIES FOR THE MICROGRID IN CASE III

Control Method	IAE	ISE	ITAE	MU	MO
W-VI	6.8463	0.7513	355.853	-0.3205	0.1972
T-VI	6.8150	0.6943	357.646	-0.2823	0.1738
COA-VI	1.6389	0.0530	79.271	-0.1479	0.0842
GAPI+VI	0.0041	2.00e-06	0.1670	-0.0021	0.001
OFOPI+VI	0.0038	1.98e-06	0.1531	-0.0019	0.001
ONFOPI+VI	0.0028	1.00e-06	0.1226	-0.0016	0.0007

with the COA-VI, 23.80% contrasted with the GAPI+VI control methodology, and 15.78% contrasted with the OFOPI+VI control methodology. Furthermore, regarding IAE, the ONFOPI+VI demonstrates remarkable enhancements of nearly 99.95% contrasted with the T-VI, 99.82% contrasted with the COA-VI, 31.70% contrasted with the GAPI+VI, and 26.31% contrasted with the OFOPI+VI controllers. These findings confirm the excellence of the ONFOPI+VI over the other four control methodologies studied, showcasing its ability to significantly reduce MO, MU, and IAE, thereby enhancing control precision and overall performance.

The proposed ONFOPI+VI control methodology also demonstrated a noteworthy reduction of 50.00% in ISE, 28.65% in IAE, 11.11% in the MU, and 46.15% in MO in Case II when compared with the OFOPI+VI control methodology, highlighting its superior performance and efficacy across diverse scenarios and metrics.

In the first case, the ONFOPI+VI control methodology showed notable advancements of roughly 99.95% contrasted with the T-VI, 99.84% contrasted with the COA-VI, 38.87% contrasted with the GAPI+VI, and 32.84% contrasted with the OFOPI+VI controller in terms of ITAE.

VI. Conclusion

This study introduced an innovative ONFOPI+VI control methodology to enhance frequency stability in low-inertia islanded microgrids. By integrating nonlinear fractional-order PI control with virtual inertia and damping mechanisms, the approach effectively manages energy storage systems and addresses uncertainties in renewable generation. The proposed controller was optimized using the COA algorithm, demonstrating significant improvements in system performance. Simulation results demonstrated that the ONFOPI+VI controller outperformed conventional methods, achieving at least a 30% improvement in IAE, a 22% reduction in MU, and a 20% improvement in ITAE. The proposed approach is adaptable to varying renewable generation levels and offers a robust solution for dynamic stability. Future research could explore hybrid controllers combining intelligent and fractional-order strategies, integrate electric vehicle batteries as mobile energy storage, and assess the real-time implementation of the ONFOPI+VI methodology, with a focus on communication delays and practical applicability.

References

[1] E. S. Parizy, S. Choi, and H. R. Bahrami, "Grid-Specific Co-Optimization of Incentive for Generation Planning in Power Systems With Renewable Energy Sources," *IEEE Transactions on Sustainable Energy,* Vol. 11, no. 2, pp. 947-957, 2020.

[2] Y. Li, M. Han, M. Shahidehpour, J. Li, and C. Long, "Data-driven distributionally robust scheduling of community integrated energy systems with uncertain renewable generations considering integrated demand response," *Applied Energy*, Vol. *335*, p. 120749, 2023.

[3] S. Jain, R. K.Ahuja, , A. Gupta, Y. Arya, "Hybrid intelligent h-AFSA-ANN controller for the SPV-BESS-DG-based DC microgrid integrated system," *Electrical Engineering*, pp. 1-26, 2024.

[4] M. El-Hendawi, H. A. Gabbar, G. El-Saady, and E.-N. A. Ibrahim, "Control and EMS of a Grid-Connected Microgrid with Economical Analysis,"*Energies,*Vol. 11, no. 1, p.129, 2018.

[5] M. Deepak, R. J. Abraham, F. M. Gonzalez-Longatt, D. M. Greenwood, and H.-S. Rajamani, "A novel approach to frequency support in a wind integrated power system," *Renewable Energy,* Vol. 108, pp. 194-206, 2017.

[6] A. Khazali, N. Rezaei, H. Saboori, and J. M. Guerrero, "Using PV systems and parking lots to provide virtual inertia and frequency regulation provision in low inertia grids," *Electric Power Systems Research,* Vol. 207, p. 107859, 2022.

[7] S. M. Said, M. Aly, B. Hartmann, and E. A. Mohamed, "Coordinated fuzzy logic-based virtual inertia controller and frequency relay scheme for reliable operation of low-inertia power system," *IET Renewable Power Generation,* Vol. 15, no. 6, pp. 1286-1300, 2021.

[8] B. Khokhar and K. P. S. Parmar, "A novel adaptive intelligent MPC scheme for frequency stabilization of a microgrid considering SoC control of EVs," *Applied Energy,* Vol. 309, p. 118423, 2022.

[9] T. Mahto, R. Kumar, H. Malik, S. M. S. Hussain, and T. S. Ustun, "Fractional Order Fuzzy Based Virtual Inertia Controller Design for Frequency Stability in Isolated Hybrid Power Systems," *Energies,* Vol. 14, no. 6, p. 1634, 2021.

[10] [G. Magdy, H. Ali, and D. Xu, "A new synthetic inertia system based on electric vehicles to support the frequency stability of low-inertia modern power grids," *Journal of Cleaner Production,* Vol. 297, p. 126595, 2021.

[11] P. Saxena, N. Singh, and A. K. Pandey, "Enhancing the dynamic performance of microgrid using derivative controlled solar and energy storage based virtual inertia system," *Jour. of Energy Storage,* Vol. 31, p. 101613, 2020.
[12] A. Fernández-Guillamón, E. Gómez-Lázaro, E. Muljadi, and Á. Molina-García, "Power systems with high renewable energy sources: A review of inertia and frequency control strategies over time," *Renewable and Sustainable Energy Reviews,* Vol. 115, p. 109369, 2019.
[13] M. Dreidy, H. Mokhlis, and S. Mekhilef, "Inertia response and frequency control techniques for renewable energy sources: A review," *Renewable and Sustainable Energy Reviews,* Vol. 69, pp. 144-155, 2017.
[14] K. S. Ratnam, K. Palanisamy, and G. Yang, "Future low-inertia power systems: Requirements, issues, and solutions - A review," *Renewable and Sustainable Energy Reviews,* Vol. 124, p. 109773, 2020.
[15] M. Sajadinia, "An adaptive virtual inertia control design for energy storage devices using interval type-2 fuzzy logic and fractional order PI controller," *Journal of Energy Storage,* Vol. 84, p. 110791, 2024.
[16] K. Komala, K. P. Kumar, and S. H. C. Cherukuri, "Storage and non-Storage Methods of Power balancing to counter Uncertainty in Hybrid Microgrids - A review," *Journal of Energy Storage,* Vol. 36, p. 102348, 2021.
[17] J. Liu, Z. Yang, J. Yu, J. Huang, and W. Li, "Coordinated control parameter setting of DFIG wind farms with virtual inertia control," *International Journal of Electrical Power & Energy Systems,* Vol. 122, p. 106167, 2020.
[18] E. Unamuno, J. Paniagua, and J. A. Barrena, "Unified Virtual Inertia for ac and dc Microgrids: And the Role of Interlinking Converters," *IEEE Electrification Magazine,* Vol. 7, no. 4, pp. 56-68, 2019.
[19] G. Magdy, G. Shabib, A. A. Elbaset, and Y. Mitani, "A novel coordination scheme of virtual inertia control and digital protection for microgrid dynamic security considering high renewable energy penetration," *IET Renew. Power Gener.,* Vol. 13, no. 3, pp. 462-474, 2019.
[20] R. Mandal and K. Chatterjee, "Virtual inertia emulation and RoCoF control of a microgrid with high renewable power penetration," *Electric Power Systems Research,* Vol. 194, p. 107093, 2021.
[21] T. Kerdphol, F. S. Rahman, Y. Mitani, M. Watanabe, and S. K. Küfeoğlu, "Robust Virtual Inertia Control of an Islanded Microgrid Considering High Penetration of Renewable Energy," *IEEE Access,* Vol. 6, pp. 625-636, 2018.
[22] A. Fathi, Q. Shafiee, and H. Bevrani, "Robust Frequency Control of Microgrids Using an Extended Virtual Synchronous Generator," *IEEE Transactions on Power Systems,* Vol. 33, no. 6, pp. 6289-6297, 2018.
[23] S. Asgari, A. A. Suratgar, and M. Kazemi, "Feedforward Fractional Order PID Load Frequency Control of Microgrid Using Harmony Search Algorithm," *Iranian Journal of Science and Technology, Transactions of Electrical Engineering,* Vol. 45, no. 4, pp. 1369-1381, 2021.
[24] A.X.R. Irudayaraj, N.I.A. Wahab, M.G. Umamaheswari, M.A.M. Radzi, N.B. Sulaiman, V. Veerasamy, S.C. Prasanna, and R. Ramachandran, "A Matignon's Theorem Based Stability Analysis of Hybrid Power System for Automatic Load Frequency Control Using Atom Search Optimized FOPID Controller," *IEEE Access,* Vol. 8, pp. 168751-168772, 2020.
[25] A. Fathy, D. Yousri, H. Rezk, S. B. Thanikanti, and H. M. Hasanien, "A Robust Fractional-Order PID Controller Based Load Frequency Control Using Modified Hunger Games Search Optimizer," *Energies,* Vol. 15, no. 1, p. 361, 2022.
[26] A.-A. Zamani, M. Shafiee, and M. Sajadinia, "Optimal self-tuning fractional order fuzzy load frequency control considering sustainable energy sources and electric vehicle," *International Journal of Ambient Energy,* pp. 1-15, 2023.
[27] Y. Arya, R. Ahmad, I. Nasiruddin, and M. F. Ahmer, "LFC performance advancement of two-area RES penetrated multi-source power system utilizing CES and a new CFOTID controller," *Journal of Energy Storage*, Vol.*87*, p.111366., 2024.
[28] K. Hongesombut and R. Keteruksa, "Fractional order based on a flower pollination algorithm PID controller and virtual inertia control for microgrid frequency stabilization," *Electric Power Systems Research,* Vol. 220, p. 109381, 2023.
[29] S.A. Zaid, A. Bakeer, G. Magdy, H. Albalawi, A.M. Kassem, M.E. El-Shimy, H. AbdelMeguid, and B. Manqarah, "A new intelligent fractional-order load frequency control for interconnected modern power systems with virtual inertia control," *Fractal and Fractional,* Vol. 7, no. 1, p. 62, 2023.
[30] R. Mandal and K. Chatterjee, "Design of a maiden synthetic inertia controller using super-capacitor energy storages and electric vehicles and real-time validation of the performance of the controller," *Journal of Energy Storage,* Vol. 55, p. 105559, 2022.
[31] C. A. Monje, Y. Chen, B. M. Vinagre, D. Xue, and V. Feliu-Batlle, *Fractional-order systems and controls: fundamentals and applications*. Springer Science & Business Media, 2010.
[32] I. Petráš, *Fractional-order nonlinear systems: modeling, analysis and simulation*. Springer Science & Business Media, 2011.
[33] T. Kerdphol, FS. Rahman, M. Watanabe, and Y. Mitani, Virtual inertia synthesis and control. Cham, Switzerland, Springer, 2021.
[34] I. Naruei and F. Keynia, "A new optimization method based on COOT bird natural life model", *Expert Systems with Applications*, Vol. *183*, p. 115352, 2021.
[35] A. Oustaloup, La commande CRONE: commande robuste d'ordre non entier. Hermes. 1991.
[36] P. Shah, and S. Agashe, "Review of fractional PID controller", *Mechatronics*, Vol. *38*, pp. 29-41, 2016.
[37] I. Petráš, "A note on fractional-order non-linear controller: possible neural network approach to design". In *2016 International Joint Conference on Neural Networks (IJCNN)*, 2016, IEEE, pp. 603-608.
[38] I. Petráš, "Tuning of the non-linear fractional-order controller". In *2019 20th International Carpathian Control Conference (ICCC),* 2019, IEEE, pp. 1-4.

Appendix A

Microgrid Control System: $H = 0.083 P.U.MWs$, $D=0.015\ P.U.\ MW/Hz$; Inertia Control: $T_{INV} = 10s$, $P_{ESS}^{U} = 0.3\ P.U.MW$, $P_{ESS}^{L} = -0.3\ P.U.MW$; Primary Control: $R = 2.4\ Hz/P.U.MW$, $T_g = 0.1s$, $T_t = 0.4\ s$, $GRC= 20\%$, $V_U = 0.3\ P.U.MW$, $V_L = -0.3\ P.U.MW$; Secondary Control: $\beta = 1.0\ P.U.MW/Hz$, $K_s = 0.05$; Renewable Energy Sources: $T_{WT} = 1.5s$, $T_{PV} = 1.8s$

Abbas-Ali Zamani was born in 1986 in Isfahan, Iran. He earned a B.Sc. degree in electronic engineering from Hakim Sabzevari University in Iran in 2009, and an M.Sc. degree in control engineering from Isfahan University of Technology in 2011. In 2018, he received his Ph.D. in control engineering from the University of Sistan and Baluchestan in Iran. Dr. Zamani is currently an assistant professor in the Department of Electrical Engineering, National University of Skills (NUS), Tehran, Iran and Technical and Vocational University (TVU) , Tehran, Iran. Seismic control, power system control, smart grids, renewable energies, and artificial intelligence are among his research interests.